Resonance structure of $^{32}S+n$ from measurements of neutron total and capture cross sections

J. Halperin, C. H. Johnson, R. R. Winters,* and R. L. Macklin
Oak Ridge National Laboratory, Oak Ridge, Tennessee 37830
(Received 2 October 1979)

Neutron total and capture cross sections of ^{32}S have been measured up to 1100 keV neutron energy [$E_{exc}(^{33}S) = 9700$ keV]. Spin and parity assignments have been made for 28 of the 64 resonances found in this region. Values of total radiation widths, reduced neutron widths, level spacings, and neutron strength functions have been evaluated for $s_{1/2}$, $p_{1/2}$, $p_{3/2}$, and $d_{5/2}$ levels. Single particle contributions using the valency model account for a significant portion of the total radiation width only for the $p_{1/2}$-wave resonances. A significant number of resonances can be identified with reported levels excited in $^{32}S(d,p)$ and $^{29}Si(\alpha,n)$ reactions. A calculation of the Maxwellian average cross section appropriate to stellar interiors indicates an average capture cross section at 30 keV, $\bar{\sigma} \simeq 4.2(2)$ mb, a result that is relatively insensitive to the assumed stellar temperature. Direct (potential) capture and the s-wave resonance capture contributions to the thermal capture cross section do not fully account for the reported thermal cross section (530 ± 40 mb) and a bound state is invoked to account for the discrepancy.

[NUCLEAR REACTIONS $^{32}S(n,n)$, $E_n = 25$–1100 keV, $^{32}S(n,\gamma)$ $E_n = 2.5$–1100 keV; measured $\sigma_{n,tot}(E)$, $\sigma_{n,\gamma}$; deduced level properties, l, J, π, $\langle E_0, \Gamma_n, \Gamma_\gamma \rangle$; calc avg properties: $\langle D_{lJ} \rangle$, $\langle S_{lJ} \rangle$ for $l = 0$, 1, 2; calc single particle contribution to Γ_γ (Valency model); calc Maxwellian avg cross sections.]

I. INTRODUCTION

Although neutron reactions on ^{32}S are of interest in some nuclear reactor applications, astrophysical modeling, and the study of single-particle effects, the available data are incomplete. There are several studies over limited energy regions[1-6] of σ_{tot} for sulfur (95% ^{32}S); however, only Peterson *et al.*[7] and Cierjacks *et al.*[8] cover a substantial portion of the energy spectrum. Peterson's 1950 work with typical $^7Li(p,n)$ resolution detected only the most prominent resonances. The data of Cierjacks are of relatively high quality, but start only at 500 keV. Neither study included analyses of resonance parameters. The capture cross section σ_γ (^{32}S) has been studied even less than the total cross section. Only the region below the 102.7 keV resonance has been investigated[6,9] including several studies of nonthermal neutron capture gamma-ray spectra.[10-12]

The measurements of both neutron capture and total cross sections complement each other. In the present work all definite assignments of resonance J values and total widths are deduced from the total cross sections. The capture cross section experiments give the kernel ($g\Gamma_n\Gamma_\gamma/\Gamma$) from which Γ_γ can be found given $g\Gamma_n$ from the transmission measurements, although the total width may sometimes also be evaluated from the capture data provided that the resonance is not too narrow compared to the resolution (e.g., >20%). The neutron capture experiments tend to be somewhat more sensitive to detecting resonances of higher l value than do the total cross section measurements; 13 resonances are reported here that were seen only in the capture work.

II. TRANSMISSION MEASUREMENTS

The total cross sections of sulfur (see Figs. 1 and 2) were measured in a time of flight transmission experiment for which the Oak Ridge Electron Linear Accelerator (ORELA) was pulsed at 800 bursts/s with a nominal burst width of 5 ns. The resulting neutron burst has a continuous spectrum produced by the photoneutron process in tantalum with subsequent moderation in a 15 cm diameter beryllium clad water target. This target is 3.2 cm thick in the direction of the flight path. Neutrons were detected by proton recoil in a 2 cm thick NE-110 scintillator placed at the end of a nominal 200 m evacuated flight path. The path length has been measured by a steel tape under controlled temperature and tension such that the distance between centers of the source and detector is known to ±5 mm; a total uncertainty of ±10 mm is assigned to allow for the additional uncertainties in the effective centers for neutron production and detection.

By means of a digital time analyzer the arrival of each detected neutron was measured to ±1 ns relative to the arrival of the gamma-ray burst at the detector. Total neutron flight times are determined by adding the gamma-ray flight time to this relative time, and the neutron energies are calculated relativistically. Data were collected

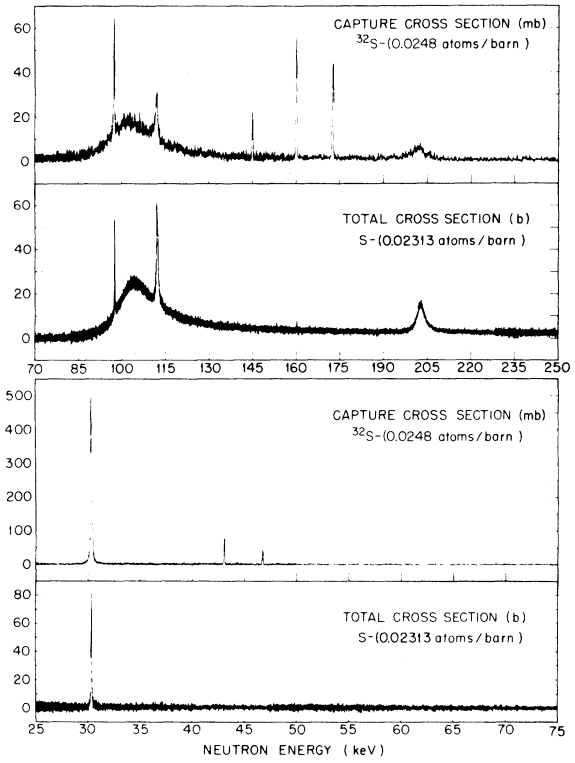

FIG. 1. A comparison of total and effective capture cross sections to 250 keV.

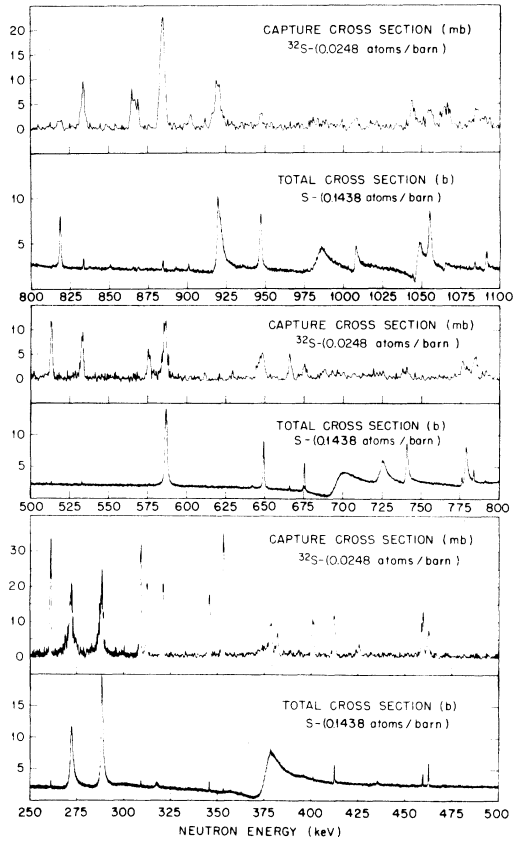

FIG. 2. A comparison of total and effective capture cross sections from 250 to 1100 keV.

in 40 000 time channels. All counts were corrected for the precise 1104 ns deadtime in the digital time analyzer; the maximum correction was 22%. Most channel widths were set at 1 to 4 ns in order to give at least five channels per resolution width; however, data at energies below 47 keV were obtained with 8 ns channels such that there were only 2.5 channels per width at some low energies. The neutron energy resolution function is expected to be a combination in quadrature of the variations in flight path and flight time. Thus,

$$(\Delta E/E)^2 = (a + bE) \times 10^{-6},$$

where ΔE is the full width at half maximum of a Gaussian resolution function. Measurements and analyses[13] of narrow resonances in Ca have shown that the respective values of a and b are 0.23 and 0.74 for $E < 0.6$ MeV and $a = 0.43$, $b = 0.41$ for $E > 0.6$ MeV. Typical values of ΔE from this expression are 55 eV at 100 keV and 900 eV at 1 MeV.

Four components of background have been identified: (a) constant room background, (b) 2.23 MeV gamma rays which are generated by capture in hydrogen at the source and decay with a 17 μs half-life, (c) 0.478 MeV gamma rays from the ^{10}B$(n, \alpha\gamma)$ reaction in the pyrex face of the detector phototube, and (d) small delayed pulses associated with the gamma burst. The last of these was reduced by placing a uranium filter in the neutron beam and by gating the detector on only after the gamma burst, except when measuring the gamma burst itself. To facilitate the measurement and subtraction of the backgrounds, data were recorded for four contiguous ranges of pulse height. Thus the higher pulse height data could be discarded for low neutron energies without loss of proton recoil data and the signal to background ratio at high neutron energies could be improved by using only the higher pulse height data. A thin ^{10}B filter was used to ensure that the counting rate after each burst had fallen to room background before the arrival of the next burst. With the sample out, the background was less than 1%, usually about 0.1% for $E > 50$ keV. Further experimental details are given elsewhere.[14]

Most of the transmissions were measured for a sulfur sample with 0.1438 atoms/b; but a thinner sample, 0.02313 atoms/b, was used also to obtain data at low energy resonances. In each case the incident neutron flux was monitored with a fission counter and the sample was oscillated in and out

of the beam about 100 times during the experiment to minimize effects of possible variations in the flux.

Total cross sections obtained with the thin and thick samples are shown respectively in Fig. 1 (25 to 250 keV) and Fig. 2 (250 to 1100 keV). All channels are plotted without averaging. The steps in channel widths are evident from the abrupt changes in statistical variations; these occur at 47 keV (8 to 4 ns channels), at 82 keV (4 to 2 ns), and at 228 keV (2 to 1 ns). The thinner sample data in Fig. 1 were necessary for the 30-, 97-, and 112-keV resonances, but the data from the thick sample had the better statistics and were used for most of the evaluation in this energy region as well as at higher energies.

III. ANALYSIS OF THE TRANSMISSION

We have analyzed the resonances in transmission by least squares fitting in terms of the R-matrix formalism including the experimental effects of Doppler and resolution broadening. In principle, this could have been done with the complete multilevel multichannel formalism over the entire energy region from 25 to 1100 keV. Actually we have analyzed each resonance by the single-level formalism, but we emphasize that this formalism retains the most important contributions of other levels. It is not a single-level approximation in which the effects of other levels are completely neglected. Thus, the deduced parameters, properly interpreted, can be inserted into the multilevel expressions to produce an essentially correct description of the cross sections including level-level interference.

The total cross section is an incoherent sum over total and orbital angular momentum quantum numbers J and l. Lane and Thomas[15] have shown that for each J, l the total neutron cross section near a level with neutron eigenenergy E_i and total width $\Gamma=\Gamma_n+\Gamma_\gamma+\Gamma_\alpha$ can be written

$$\sigma^{Jl}(E)=\sigma^{Jl}_{nn}(E)+\sigma^{Jl}_{n\gamma\alpha}(E)\,, \tag{1a}$$

where

$$\sigma^{Jl}_{nn}=4\pi k^{-2}g_J\left|(\Gamma_n/\Gamma)\exp(i\delta_{Jl})\sin\delta_{Jl}+\exp(-i\phi'_{Jl})\sin\phi'_{Jl}\right|^2 \tag{1b}$$

for elastic scattering, and

$$\sigma^{Jl}_{n\gamma\alpha}=\pi k^{-2}\,g_J\,\frac{\Gamma_n(\Gamma_\gamma+\Gamma_\alpha)}{(E_i+\Delta_i-E)^2+(\Gamma/2)^2} \tag{1c}$$

is the absorptive term. The statistical factor g_J is $(2J+1)/2(2I+1)$ where I is the spin of the target. The absorptive term is written as an approximation in which the contribution of other levels is neglected; however, the elastic term includes the interference with all other levels. The resonance phase shift δ_{Jl} is given by

$$\delta_{Jl}=\tan^{-1}[(\Gamma/2)/(E_i+\Delta_i-E)]\,, \tag{2}$$

where Γ_n, Δ_i, and ϕ'_{Jl} are each modified by the R function for all levels excluding level i, namely,

$$R^0_{Jl}=\sum_{\lambda\neq i}\gamma_\lambda{}^2/(E_\lambda-E)\,, \tag{3}$$

where $\gamma_\lambda{}^2$ is the reduced neutron width of the level at E_λ. This reduction of the R matrix to a single element, an R function, follows from the approximation that the off-diagonal elements of R^0_{Jl} are zero (i.e., the random phase approximation). The "potential" phase is

$$\phi'_{Jl}=\phi_l+\tan^{-1}(R^0_{Jl}P_l)\,, \tag{4}$$

where ϕ_l is the hard sphere scattering phase angle.

We choose the boundary condition B_l equal to the shift factor S_l at each resonance so that neither appears explicitly in the formulation. The expressions for Γ_n and Δ_i can then be written[15]

$$\Gamma_n=2P_l\gamma_i{}^2/d_{Jl}$$

and

$$\Delta_i=\gamma_i{}^2P_l{}^2R^0_{Jl}/d_{Jl}\,, \tag{5}$$

where

$$d_{Jl}=1+(P_lR^0_{Jl})^2\,.$$

The channel radius must be chosen beyond the range of the nuclear polarizing forces. We have chosen $a_c=6.4$ fm, a radius where a Woods-Saxon form for the nuclear potential is less than 2% of its central value. The penetrabilities P_l are calculated using this value for a_c.

In addition to Γ_n we report Γ^l_n, which by convention is Γ_n "reduced" to its value at 1 eV in the laboratory. However, for our energy region we define Γ^l_n more nearly completely than has been the convention at lower energies

$$\Gamma^l_n=d_{Jl}\Gamma_n\left(\frac{1\text{ eV}}{E_0(\text{eV})}\right)^{1/2}\frac{(ka_c)}{P_l}\,, \tag{6}$$

where $k=b\sqrt{E(\text{eV})}$ and $b=(0.219\,68\times10^{-3})\times A(A+1.0087)^{-1}$. These "reduced" widths are directly proportional to the R-matrix reduced width $\gamma_\lambda{}^2$,

$$\Gamma^l_n=2ba_c\gamma_\lambda{}^2\,. \tag{7}$$

Conventionally the factor d_{Jl} in Eq. (6) has been approximated by unity. That is a good approximation for higher l values or at very low energies for s waves such that the penetrabilities are small enough to make $R^0_{Jl}P_l$ negligible in d_{Jl}. But at the energies of the present work the correct d_{Jl} should

TABLE I. Resonance parameters and spin-parity assignments for $^{32}S+n$.

E_0 (keV)	$\left(\frac{g\Gamma_n}{\text{resolution}}\right)$	$g\Gamma_n$ (eV)	Γ_γ (eV)	ϕ' (rad)	J^π or l
30.380 (5)	4.2	63.6 (11)	1.01 (5)	+0.01 (1)	$\frac{1}{2}^-$
43.103 (15)	...	<1	0.076 (5) [a]	...	($l=2$)
46.790 (15)	...	<1	0.050 (4) [a]	...	($l=2$)
97.500 (11)	4.4	234 (4)	0.29 (2)	+0.00 (1)	$\frac{3}{2}^-$
102.71 (2)	270	15000 (100)	7.0 (15)	−0.260 (5)	$\frac{1}{2}^+$
112.18 (2)	18	1116 (10)	0.38 (3)	−0.02 (1)	$\frac{3}{2}^-$
145.14 (7) [b]	...	<3	0.27 (2) [c]	...	
160.20 (2)	0.10	9.4 (5)	1.02 (7) [c]	−0.01 (2)	$l=1,2$
172.70 (7) [b]	...	<4	0.89 (5) [c]	...	
202.63 (3)	24	3050 (20)	0.90 (10)	−0.063 (5)	$\frac{1}{2}^-$
261.08 (3)	0.088	15 (1)	1.56 (10) [c]	+0.01 (4)	$l>0$
272.08 (4)	9.3	1660 (10)	4.06 (30)	−0.110 (10)	$\frac{1}{2}^-$
288.38 (4)	12	2240 (30)	1.82 (15)	−0.073 (5)	$\frac{3}{2}^-$
309.13 (4)	0.090	19 (1)	2.53 (20) [c]	−0.01 (4)	$l>0$
312.34 (5)	0.019	4 (1)	1.91 (15) [c]	−0.2 (2)	
321.10 (10) [b]	...	<9	1.76 (15) [c]	...	
345.74 (5)	0.18	43 (2)	1.72 (15) [c]	−0.04 (3)	$l>0$
353.23 (5)	0.072	18 (2)	3.87 (30) [c]	−0.10 (6)	$l>0$
376.55 (5)	29	7850 (30)	2.18 (55)	−0.532 (5)	$\frac{1}{2}^+$
378.52 (10)	0.055	15 (5)	0.91 (12) [c]	...	
382.10 (15) [b]	...	<11	0.65 (10) [c]	...	
401.11 (7)	0.051	15 (2)	1.52 (12) [c]	...	
412.33 (6)	0.48	145 (5)	0.90 (8)	−0.10	$\frac{3}{2}^-$
425.80 (20) [b]	...	<12	0.46 (10) [c]	...	
459.67 (6)	0.30	105 (5)	2.03 (20) [c]	+0.07 (2)	$l>1$
462.76 (6)	0.69	244 (5)	0.44 (5)	+0.07 (1)	$\frac{5}{2}^+$
513.33 (12)	0.060	24 (5)	2.79 (25) [c]	+0.0 (2)	$l>0$
532.97 (10)	0.071	30 (3)	2.48 (25) [c]	+0.0 (2)	$l>0$
576.04 (25) [b]	...	<17	1.72 (25) [c]	...	
586.08 (12)	0.48	300 (50)	2.8 (28) [c]	0.0 [d]	$l>0$
586.88 (10)	8.1	3860 (50)	0.9 (9)	0.0 (1)	$\frac{5}{2}^+$
645.5 (5) [b]	...	<20	0.7 (2) [c]	...	
649.24 (10)	2.6	1420 (15)	1.04 (17)	−0.01 (1)	$\frac{5}{2}^+$
665.98 (13)	0.13	72 (8)	1.37 (15) [c]	0.0 (2)	$l>0$
675.37 (10)	1.4	790 (10)	0.40 (12)	−0.01 (1)	$\frac{5}{2}^+$
687.8 (10) [b]	...	<22	0.86 (25) [c]	...	
696.04 (12)	20	11800 (120)	2.0 (10)	−0.69 (1)	$\frac{1}{2}^+$
724.79 (11)	7.3	4500 (50)	0.9 (3)	−0.28 (1)	$\frac{1}{2}^-$
738.0 (5) [b]	...	<24	0.4 (2) [c]	...	

TABLE I. *(Continued.)*

E_0 (keV)	$\left(\frac{g\Gamma_n}{\text{resolution}}\right)$	$g\Gamma_n$ (eV)	Γ_γ (eV)	ϕ' (rad)	J^π or l
740.85 (12)	3.5	2240 (25)	0.4 (1)	−0.18 (1)	$\frac{3}{2}^-$
776.3 (2)	0.29	196 (10)	1.5 (2) [c]	···	$l>0$
778.65 (12)	4.3	2880 (30)	0.3 (1)	−0.23 (1)	$\frac{3}{2}^-$
783.80 (13)	0.37	250 (10)	2.6 (3) [c]	+0.04 (4)	$l>1$
818.72 (13)	2.4	1690 (20)	0.4 (1)	0.00 (1)	$\frac{5}{2}^+$
833.73 (14)	0.30	220 (12)	5.5 (4) [c]	+0.08 (8)	$l>1$
865.6 (4)	0.065	50 (20)	3.9 (4) [c]	0.0 (4)	$l>0$
868.8 (4)	0.10	80 (10)	3.4 (5) [c]	0.0 (4)	$l>0$
884.59 (15) [e]	0.331	260 (25)	17.0 (10) [c]	+0.03 (4)	$l>1$
901.12 (16)	0.16	130 (20)	1.4 (3) [c]	+0.03 (7)	$l>1$
910.5 (5) [b]	···	<30	0.5 (2) [c]	···	
919.87 (15)	2.9	2415 (70)	0.8 (8)	0.0 [d]	$\frac{5}{2}^+$
920.88 (16)	6.7	5550 (100)	1.3 (13)	−0.23 (1)	$\frac{3}{2}^-$
947.26 (16)	3.6	3090 (30)	0.8 (2)	0.00 (1)	$\frac{5}{2}^+$
984.99 (21)	9.3	8300 (100)	3.0 (10)	−0.32 (2)	$\frac{1}{2}^-$
1007.8 (2)	0.23	210 (70)	0.6 (6) [c]	>−0.3 [d]	$l>0$
1007.8 (2)	1.4	1550 (150)	0.6	−0.48 (5)	$\frac{1}{2}^-$
1044.8 (2)	0.21	200 (100)	4.9 (6) [c]	0.0 [d]	$l>0$
1046.5 (3)	2.2	2100 (300)	0.5 (5)	−0.80 [d]	$\frac{1}{2}^+$
1048.5 (3)	2.6	2500 (300)	0.5 (5)	−0.38 (10)	$\frac{1}{2}^-$
1055.3 (2)	4.0	3900 (100)	1.2 (3)	−0.03 (1)	$\frac{5}{2}^+$
1062 (1) [b]	···	<37	2.6 (10) [c]	···	
1064.9 (2)	0.31	305 (100)	3.0 (12)	−1.0 (1)	$\frac{1}{2}^+$
1084.2 (2)	0.24	245 (30)	4.0 (10) [c]	−0.06 (4)	$l>1$
1091.4 (2)	0.80	820 (40)	0.5 (3)	−0.25 (2)	$\frac{3}{2}^-$

[a] $g\Gamma_n\Gamma_\gamma/\Gamma = g\Gamma_n$; the kernel measures $g\Gamma_n$.
[b] Seen in capture only. Upper bound given for $g\Gamma_{\text{Tot}}$.
[c] $g\Gamma_n\Gamma_\gamma/\Gamma$, the capture kernel.
[d] Potential phase fixed.
[e] Possible multiplet.
[f] Background slope set to zero.

be included, particularly for s waves, to maintain the proportionality of the conventional widths to the γ_λ^2 of the R-matrix formalism. For the s-wave resonances at 696, 1046, and 1065 keV for example, d_{Jl} is 1.23, 1.46, and 1.18, respectively. This variation in d_{Jl} reflects the Porter-Thomas width fluctuations of the nearby levels included in R^0_{Jl}.

For later interpretation we also introduce an average R function $\bar{R}_{Jl}$ (as defined by Lane and Thomas[15]) which removes the Porter-Thomas fluctuations by means of a continuous strength function $s_{Jl}(E)$,

$$\bar{R}_{Jl}(E) = \Pr \int_{-\infty}^{\infty} dE' s_{Jl}(E')/(E'-E), \tag{8}$$

where Pr signifies "principal part of."

A program DCON was written to fit by least squares either one level or two levels of different Jl. The alpha-particle widths were neglected and the Γ_γ were assigned from the capture data. The adjustable parameters include two for a linear background plus a J, Γ_n, E_0, and ϕ'_{Jl} (for each resonance). Here J must be a half-integer and E_0 replaces $E_i+\Delta_i$. To formulate the com-

puter program we note that three terms result when Eq. (1b) is expanded. The first is a symmetric Breit-Wigner term to which the absorptive term is to be added. The second shows unsymmetric interference which depends strongly on ϕ'_{Jl}. The third is a cross section, proportional to $\sin^2\phi'_{Jl}$, that would occur if the resonance i were not present; it can be treated as a background to be added to that from all other Jl channels and to the contributions of the minor isotopes. This total nonresonant background is approximated as linear in energy; thus, an important energy dependence of ϕ'_{Jl} for other levels is included in the analysis of each individual level. For the Breit-Wigner and interference terms, the energy dependence of Γ_n, E_0, and ϕ'_{Jl} resulting from the penetrability and hard-sphere phase are included if necessary, i.e., for the broad s-wave resonances; but the dependences on other levels are approximated as constant. In other words, R^0_{Jl} is assumed to be constant over the width of the resonance except in the background $\sin^2\phi'_{Jl}$ terms. From the "single-level" parameters thereby derived one can deduce multilevel parameters by the foregoing equations. This subject will be treated in a later paper.

Table I lists 64 resonances of which 51 were observed in transmission. Here we discuss only the transmission resonances, all of which were analyzed by the least squares fitting program. Column 1 lists each resonance energy E_0 with its uncertainty. The uncertainty includes the statistical uncertainty (as evaluated by the fitting program) but is usually dominated by the addition in quadrature of the contribution from the ±10 mm in distance plus the ±1 ns in time. (For the 30.38-keV resonance the Δt is 4 ns or half a channel.) Also listed are the best fitted values of $g\Gamma_n$ and ϕ', with associated statistical uncertainties, and the ratio $g\Gamma_n/\Delta E$, ΔE is the resolution width, for the transmission measurements. The last column gives either J^π assignments or limits on the l values deduced as discussed below.

We have assigned J^π for 28 of the levels observed in transmission. Table II lists those levels,

TABLE II. Summary of arguments supporting the J^π assignments and average valency contributions to the total radiation widths.

J^π	E_0 (keV)	J logic	π logic	Γ_n^l (eV)	d_{Jl}	Γ_γ^{obs} (eV)	$\Gamma_\gamma^v/\Gamma_\gamma^{obs}$	$\langle\Gamma_\gamma^v/\Gamma_\gamma^{obs}\rangle$
$s_{1/2}$	102.71	A	A	48.30	1.032	7.0	0.215	
	376.55	A	A	14.05	1.099	2.18	0.043	
	696.04	A	A	17.40	1.230	2.0	0.085	0.070
	1046.5	B [a]	B [a]	2.99	1.456	0.5 [a]	0.0056 [a]	
	1064.8	D	A	0.35	1.185	3.0	0.0001	
$d_{5/2}$	462.76	D	D	2.01	1.000	0.43	0.040	
	586.88	A [a]	C [a]	19.19	1.000	0.93 [a]	0.235 [a]	
	649.24	C	D	5.73	1.000	1.03	0.066	
	675.37	C	D	2.94	1.000	0.40	0.049	0.10
	818.72	C	D	4.31	1.000	0.37	0.157	
	919.87	C [a]	D [a]	4.94	1.000	0.83 [a]	0.059 [a]	
	947.26	A	D	5.98	1.000	0.67	0.134	
	1055.31	A	D	6.21	1.000	1.6	0.063	
$p_{1/2}$	30.38	A	A	6.83	1.000	1.01	0.26	
	202.63	A	A	24.77	1.000	0.90	1.35	
	272.08	A	A	9.48	1.000	4.07	0.21	
	724.79	A	A	9.21	1.000	0.90	0.66	0.50
	984.99	A	A	12.92	1.010	3.0	0.27	
	1007.8	A [a]	A [a]	2.37	1.003	0.6 [a]	0.27 [a]	
	1048.5	B [a]	B [a]	3.71	1.004	0.5 [a]	0.46 [a]	
$p_{3/2}$	97.50	A	C	2.44	1.001	0.29	0.12	
	112.18	A	C	9.66	1.000	0.37	0.37	
	288.38	A	A	5.98	1.001	1.82	0.056	
	412.33	D	A	0.26	1.003	0.89	0.006	0.13
	740.85	A	A	2.28	1.017	0.35	0.14	
	778.65	A	A	2.78	1.009	0.30	0.20	
	920.88	A [a]	A [a]	4.70	1.026	1.25 [a]	0.082 [a]	
	1091.43	D	A	0.61	1.048	0.50	0.026	

[a] Doublet.

grouped according to J^π. The columns labeled "J logic" and "π logic" are aids to the following discussion of the assignments. Each doublet member is designated by "a".

The fifteen levels with J logic $=A$ were isolated and broad enough relative to the resolution ($\Gamma/\Delta E > 1.2$) such that we easily assigned J values from the peak-to-valley difference in cross section. The assignments for the very broad levels could have been deduced by inspection, but we fitted these just as all of the rest using the parameters J, Γ_n, E_0, and ϕ' and a two parameter linear background. Actually, some of these levels were not completely isolated, but the presence of another level was not a serious problem for the single-level analysis. For example, for the 97.5- or 112.8-keV resonances the linear background accounts for the broad underlying 102.71-keV resonance. To analyze the underlying resonance itself, we simply deleted points near the two narrower peaks. Similar deletions of very narrow resonances were made for other broad resonances.

The three doublet members designated A^a are also broad ($\Gamma/\Delta E > 1.4$) but required two-level analyses to give definitive assignments. For the pairs near 587 and 921 keV the presence of the narrow member can be seen visually as an inflection on a broader resonance. Although the third pair near 1008 keV appears to be a single smooth resonance, it cannot be fitted using the single-level expression. We fitted each doublet using two noninterfering resonances. Such an analysis would be overparametrized if attacked directly using three parameters with assumed J value for each resonance plus two background parameters. Therefore for the narrower member of each doublet we fixed ϕ' (see Table I) consistently with the other phase shifts discussed below. For the doublet near 1008 keV the narrow member was restricted to $l>0$ to give consistent phases for both members of the doublet.

Figure 3 shows the cross section and fitted curve for the doublet near 587 keV. We present this doublet in particular because this resonance has been suggested as an energy standard but was not previously known to be a doublet.

Both levels designated B^a for the doublet near 1047 keV are broad, $\Gamma/\Delta E > 2.2$. Thus they are similar to the A^a group except that they overlap so completely that the number of free parameters must be further reduced. Discussion of the analysis of these is deferred to later in this section.

The four levels designated J logic $=C$ or C^a have widths between $\Delta E/2$ and ΔE for the assigned $J = \frac{5}{2}$. These cannot be fitted with $J < \frac{5}{2}$. The rejection of $J > \frac{5}{2}$ was not so definite but was adopted in each case because of the worsened quality of the fit as measured by chi-square. For the doublet member at 919.87 keV we assumed $\phi' = 0$ because both d- and f-wave phase shifts are expected to be nearly zero.

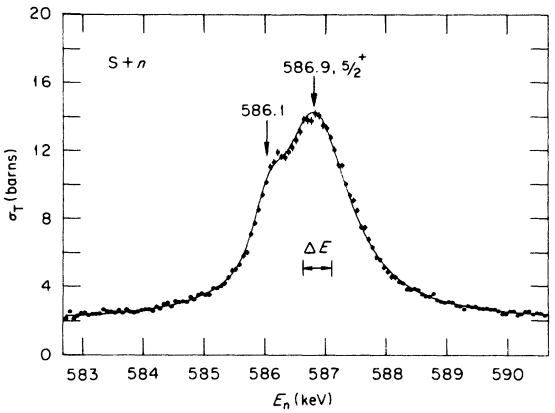

FIG. 3. The resolution of the doublet at 587 keV is illustrated. The solid curve represents the fit obtained using the DCON program.

The four levels with J logic $=D$ have $\Gamma < \Delta E/2$ for the assigned J. The J values could be larger but not smaller than the assigned value. The choice of the lowest possible J value depends on further logic, as discussed below.

We turn now to parities or l values. Our assignments are based fundamentally on the fact that both the penetrabilities and the magnitude of the nonresonance phase shifts decrease rapidly with increasing l value. In Table II the levels for which the least squares analyses yielded definite negative phases are designated π logic $=A$, A^a, or B^a. The 30.38-keV level with $J = \frac{1}{2}$ is also designated "A" even though $\phi' = 0$ because the zero phase distinguishes it from other $J = \frac{1}{2}$ levels. These phases are plotted in Fig. 4. Below we discuss the two additional $J = \frac{3}{2}$ points designated "C" that are plotted below 120 keV with nearly zero phase.

Ignoring the curves and corresponding labels (Fig. 4) for the moment, we note that the phases cluster into two groups and we conclude that the five points with systematically more negative phases must have $l=0$, whereas the rest with definite but less negative phases must have $l=1$. Calculations with any reasonable potential would give $\phi' \simeq 0$ for $l=2$ or 3. Returning to the J values, we immediately make the $s_{1/2}$, $p_{1/2}$, and $p_{3/2}$ assignments in Table II for levels having $J = \frac{1}{2}$ or $\frac{3}{2}$ with J-logic A or A^a. Levels with $J = \frac{1}{2}$ are easily classified as $p_{1/2}$ or $s_{1/2}$ and levels with $J = \frac{3}{2}$ must be $p_{3/2}$ rather than $d_{3/2}$ to account for the large negative ϕ'.

Assignment of the $s_{1/2}$-$p_{1/2}$ doublet near 1047 keV

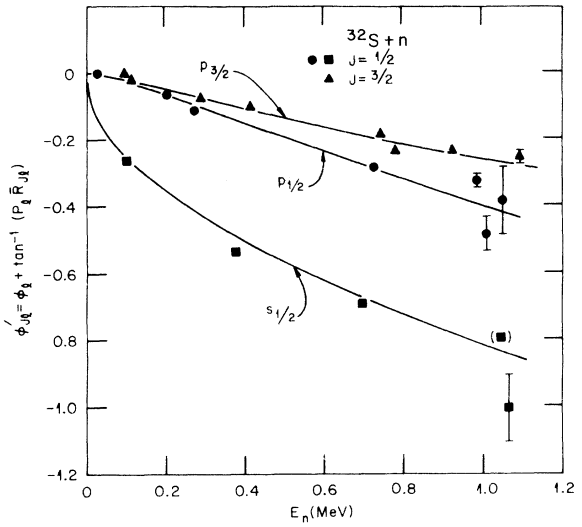

FIG. 4. The potential scattering phase angle is shown for $s_{1/2}$, $p_{1/2}$, and $p_{3/2}$ resonances. The curves are least-squares fits using a constant R function. The fluctuations about the curves primarily reflect Porter-Thomas width fluctuations.

is definite but the logic (B^a) is complicated. Figure 5 shows the transmission data to be fitted. We begin by omitting from the analysis the open circles, which are near a third narrow resonance at 1044.84 keV. The remaining data show strong interference and, at first glance, appear to result from a single resonance. In fact the fit achieved with $J = \frac{3}{2}$ has a chi-square of 1.3 per degree of freedom (the final two-level value is 0.90) but the

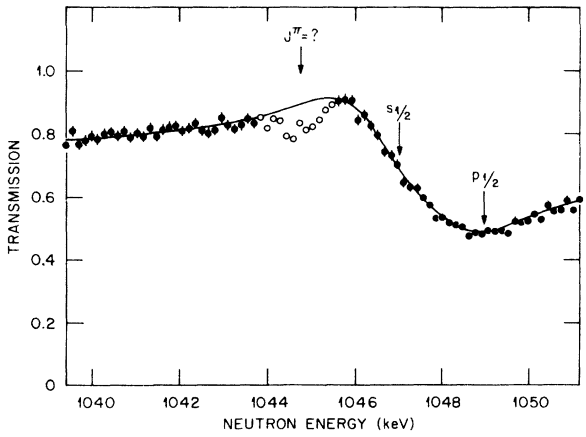

FIG. 5. Transmission for 0.1438 atom/b sulfur near the 1046.5 ($s_{1/2}$) and 1048.5 ($p_{1/2}$) keV resonances. The curve shows the two-level fit in which the s-wave phase and the slope of the background were fixed on the basis of other resonances. Data shown by open circles near the narrow 1044.8-keV resonance were omitted from this fit.

resulting ϕ' is −0.55 and is inconsistent with the other $p_{3/2}$ phases. There must be two resonances. To analyze the two resonances we must fix some of the parameters. Since a preliminary analysis showed one of the levels to have a large negative ϕ', we can assign one level $s_{1/2}$ and fix its phase consistently with the other $s_{1/2}$ resonances. To do so we return to Fig. 4.

The $s_{1/2}$ curve in Fig. 4 is obtained by fitting the R^0_{Jl} for $s_{1/2}$, corrected for the other observed $s_{1/2}$ levels using an assumed linear $\bar{R}_{Jl}$ and an assumed constant strength for 0 to 1100 keV equal to the observed average strength. The points scatter about this curve because of the fluctuation of level widths and spacings. For example, the point at 376.55 keV is relatively negative because of the influence of the broad level at 102.71 keV. Using this curve, with corrections for the observed levels, we predict $\phi' = -0.80$ rad (point in parenthesis) for the $s_{1/2}$ member of the 1047-keV doublet. Furthermore, from a multilevel calculation including all but the two levels of the doublet, we find the background to have zero slope. With these two parameters fixed we made the two-level fit shown by the curve in Fig. 5. The second level must have $J = \frac{1}{2}$ and its fitted ϕ' is consistent with the other $p_{1/2}$ resonances. Thus the analysis in terms of two $J = \frac{1}{2}$ levels of almost identical positions and widths gives a good fit with consistent phase shifts, whereas the use of a single $J = \frac{3}{2}$ level does not.

Finally we come to levels with π logic $= C$, C^a, D, or D^a for which our parities are based on the magnitudes of the neutron reduced widths rather than on ϕ', which in each case is nearly zero. We assign $p_{3/2}$ to the 97.50 and 112.18-keV levels because the other possible assignment, namely $d_{3/2}$, would lead to reduced widths of 40 to 135 times the average for the other six $p_{3/2}$ levels. That would indicate the $d_{3/2}$ strength function is at least an order of magnitude larger than for $p_{3/2}$ whereas optical model calculation suggest the opposite to be true. For the 586.88-keV resonance we assign $d_{5/2}$ because the $f_{5/2}$ assignment would give a reduced width at least 50 times the average for other levels. These are the C and C^a categories.

In like manner we assign the seven levels designated D or D^a to be d waves with the reservation, as stated below, that one of them could possibly be f wave. For d waves all seven must be $d_{5/2}$ rather than $d_{3/2}$ because the $\frac{5}{2}$ assignments are either definite or lower limits (see the J logic). With the reasonable assumption that the eight $d_{5/2}$ levels include most of the strength from 400 to 1100 keV we find a $d_{5/2}$ strength function $\langle \Gamma^I_n \rangle / \langle D \rangle$ of 0.7×10^{-4}. The corresponding $s_{1/2}$, $p_{1/2}$, and $p_{3/2}$ strengths are all similar and can be reasonably described by an optical model. But if we had as-

sumed the seven "D-logic" levels to be $f_{5/2}$ rather than $d_{5/2}$ we would have deduced an $f_{5/2}$ strength function of 6.0×10^{-4}, an order of magnitude larger than for s or p waves. Optical model calculations suggest an $f_{5/2}$ strength of only 0.3×10^{-4} or less. Therefore, we have concluded above that the seven levels cannot be all f waves. There is a small probability, however, that only one is $f_{5/2}$. If the relatively narrow 675-keV level, for example, were $f_{5/2}$, it would by itself give a strength of 0.7×10^{-4} for the 400- to 1100-keV region. Such a concentration in a single level is unlikely but cannot be ruled out.

In the upper part of Fig. 4 the $p_{1/2}$ and $p_{3/2}$ curves were each calculated using a linear R function chosen in like manner to the above $s_{1/2}$ curve to describe an average strength both inside and outside of our region. The spin-orbit splitting is apparent. As expected the $p_{1/2}$ curve is more negative than $p_{3/2}$ because the bound single-particle $p_{1/2}$ strength is closer to the neutron separation energy than is the $p_{3/2}$ strength.

The remaining 23 levels of the 51 observed in transmission and listed in Table I are not broad enough to allow definite J assignments; however, most show an interference pattern (or lack thereof) which places limits on ϕ' and, by comparison to Fig. 4, provides a lower limit on the l value. On this basis we assign $l>0$ to 14 levels and $l>1$ to six levels. In Table I the remaining three levels at 312.3, 378.5, and 401.1 keV are too narrow for any assignment.

For these 23 levels the $g\Gamma_n$ and the corresponding reduced widths place upper limits on the l values. Thus it is unlikely that any have $l=4$. However, any one except the 160.2-keV resonance could have $l=3$ without the corresponding reduced width exceeding about half of that actually observed for the 102.7-keV s-wave resonance. For the 160.2-keV resonances we assign $l<3$ or $l=1,2$ because the f-wave reduced width would be quite large, $\Gamma_n=53$ eV for $f_{5/2}$. For the others we place no upper limit except $l<4$.

The peak cross sections for the 97- and 112-keV resonances constitute the only unexplained problems encountered in analysis of the transmission measurements. These two resonances clearly have $J=\frac{3}{2}$ and should have resolution-broadened peak heights of 57.3 and 62.1 b, respectively; however, the observed peaks are only about 53.0 and 60.0 b. These discrepancies have little effect on the assigned resonance parameters; nevertheless, they are disturbing because they are not reasonably explained by the effects of backgrounds, competing reactions, resolution broadening, or the structure of the incident flux, A similar discrepancy does not occur at the 30-keV resonance or for higher energy resonances obtained with the thicker sample.

IV. AVERAGE RESONANCE PROPERTIES

The reduced neutron widths for l-wave neutrons have been evaluated using Eq. 6. The neutron strength function as conventionally defined was taken as $S_{Jl}=\langle\Gamma_n^l\rangle/\langle D_{Jl}\rangle$ (note that we use $a_c=6.4$ fm), where $\langle D_{Jl}\rangle$ is the average level spacing for resonances of the same spin and parity. The number of missed resonances has been evaluated by combining our estimate of the experimental sensitivity for the assignment of spin and parity to detected levels with an assumed Porter-Thomas distribution. Using this criterion we have estimated the number of $s_{1/2}$, $p_{1/2}$, $p_{3/2}$, and $d_{5/2}$ resonances missed (13 altogether) and have corrected average values of the reduced width, level spacing, and neutron strength function for these missing levels. In Fig. 6 are presented plots of the cumulative strength for the s- and p-wave resonances seen in

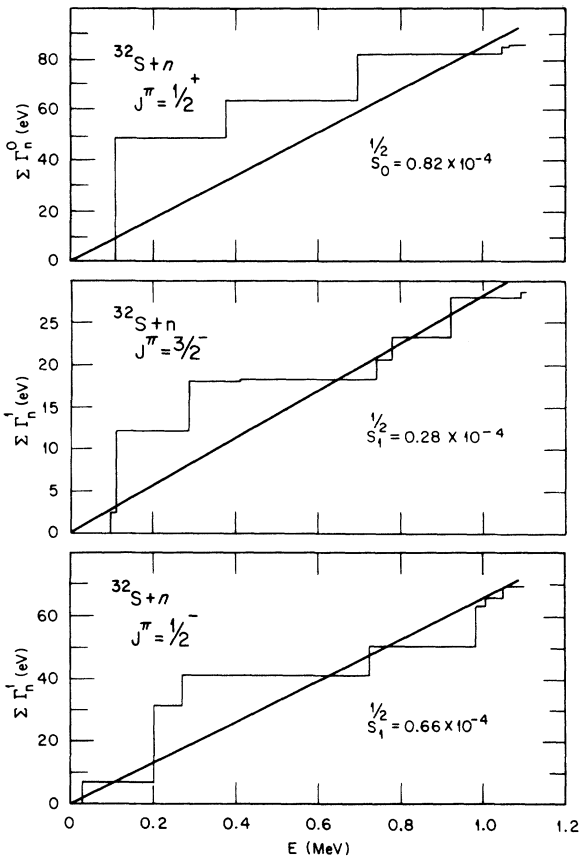

FIG. 6. A plot of the cumulative strength versus energy for $s_{1/2}$, $p_{1/2}$, and $p_{3/2}$ resonances. The heavy curve represents a least-squares fit and the derived slopes represent best estimates of the strength function.

this energy region. The cumulative plots were fitted by least squares (weighting with the fitting function); and the derived slopes represent best estimates of the strength functions for each class of resonances.

s-wave. Only five s-wave resonances have been observed in $^{32}S+n$ to 1100 keV. Assuming a Porter-Thomas distribution we estimate that there is a 5% chance of obtaining a width less than our experimental sensitivity. We estimate the average level spacing $\langle D_0\rangle = 226(60)$ keV and the neutron strength function as $\langle S_0\rangle = 0.82(55)\times 10^{-4}$ from the least-squares fit shown in Fig. 5. The value for the s-wave neutron strength function is an order of magnitude below the values for nuclides at the $3s_{1/2}$ peak[16] (near $A=50$ in the s-wave strength versus mass curve) and helps define the valley approaching the expected $2s_{1/2}$ peak where there are relatively few experimental points.

p-wave. We have identified seven $p_{1/2}$ resonances to 1100 keV and estimate that two such resonances were missed. On the basis of nine resonances, we estimate the level spacing and neutron strength function as $\langle D_{1/2,1}\rangle = 127(27)$ keV and $\langle S_{1/2,1}\rangle = 0.66(38)\times 10^{-4}$ where the uncertainties represent one standard deviation. We have identified eight $p_{3/2}$ levels and estimate that three resonances have been missed. Thus for 11 resonances we find $\langle D_{3/2,1}\rangle = 100(20)$ keV and $\langle S_{3/2,1}\rangle = 0.28(14)\times 10^{-4}$.

d-wave. Eight resonances have been assigned $\frac{5}{2}^+$ and we estimate that only about half of the $d_{5/2}$ resonances have been identified. Penetrability effects imply that only the strongest resonances will be observed below a few hundred keV. On the basis of 16 resonances, we estimate $\langle D_{5/2,2}\rangle = 70(15)$ keV and $\langle S_{5/2,2}\rangle = 0.5(3)\times 10^{-4}$.

Although the current experiment has been insensitive for identifying $d_{3/2}$ resonances, approximately 11 $\frac{3}{2}^+$ resonances can be expected on the basis of the $(2J+1)$ rule over the energy interval studied here. Thus about 52 s, p, and d resonances have either been seen or inferred from this study. This is 12 fewer than the total number observed.

V. CAPTURE MEASUREMENTS

Neutron time-of-flight measurements, see Figs. 1 and 2, were carried out with the ORELA 40 m flight path using a 4 ns wide electron beam. The neutron beam was collimated to give an approximately 2.6×5.2 cm rectangular cross section at the sample. A shadow bar in the neutron flight path several meters from the ORELA beryllium clad tantalum target attenuated the gamma flash by at least three orders of magnitude.[17] The beam used with a ^{10}B filter (0.027 atoms/b) yields an especially clean neutron spectrum. The time dependent background as determined with "black resonance" filters ranges from ~0.5% at low energies to ~1% at 1 MeV. In this experiment the time-of-flight measurements were started following a 1 μs delay after the γ flash and only one event per electron pulse was accepted. A sample of pressed natural sulfur (95% ^{32}S) of 0.0248 atoms of ^{32}S per barn was suspended in the neutron beam with 6.4 μm mylar film. The supporting film negligibly attenuated the beam and did not give rise to discernible capture gammas.

The total energy weighting technique first described by Maier-Liebnitz and developed by Macklin[18] was used to sum the energy-weighted prompt ($\lesssim 5\times 10^{-9}$ s) capture gamma-ray spectrum. The method permits the evaluation of the capture gamma cross section independent of the details of the capture gamma cascade. The γ-ray detectors were two nonhydrogeneous fluorocarbon (NE-226) scintillators (10.2 cm in diameter and 4 cm thick) placed just outside the neutron beam on each side of the sample. These detectors subtended ~55% of the 4π solid angle and had an overall detection efficiency of ~15% for a typical gamma cascade. The weighted detector response which is dominated by Compton scattering is made proportional to the total photon energy emitted by the sample. Thus the number of neutrons captured can be deduced, since each captured neutron contributes the neutron binding energy plus center of mass energy of the relative motion to a gamma cascade.

The linear pulse from the detector is digitized into 128 channels and transmitted to an on-line computer where the weight calculated for each channel is applied. These weighted values are accumulated into a series of 18 432 time-of-flight channels. The neutron energy region spanned in this measurement ranged from approximately 2.5 keV to 5 MeV (although only 1100 keV were subjected to analysis). A 0.5 mm thick ^6Li-glass neutron flux monitor is positioned in the beam 40 cm in front of the sample in transmission.[19] A plastic scintillator positioned in the beam about 7 m beyond the total energy detectors served as a flash detector and initiated the timing cycle. The digital clock using 1 ns timing channels could be stopped by a pulse from either the gamma-ray detectors or the ^6Li-glass monitor within a cycle time of 57 μs. The neutron beam was pulsed at the rate of 1000 pulses/s; the resulting maximum dead-time correction to the data was 4.3%. The Li(n,α) cross section used was that of Uttley[20] modified by more recent measurements,[21-23] especially near the 250-keV peak. Corrections have been applied for the Si, O, and Ce activator in the glass.

The 5.903- and 1094-keV peaks in the spectrum of ^{27}Al were used to calibrate the energy scale for the gamma-ray detectors, whereas the 30.38 resonance and the 586.88 keV doublet in a ^{32}S filter served to calibrate the Li-glass neutron monitor. The energy scale in capture is considered accurate to at least 0.1% over the range of energies considered here exclusive of errors in the calibrating energies of the standards that were used. The system energy resolution is dominated by the neutron moderation in the coolant water at the tantalum target at low energies and by the accelerator burst width (4 ns in this measurement) at higher energies. The time resolution of the detector is approximately 1.7 ns. The overall energy resolution ranges from 1.6×10^{-3} at 2.5 keV to 3.2×10^{-3} at 1 MeV exclusive of Doppler broadening.

The saturated resonance technique was used to calibrate the ratio of the detection efficiency of the gamma-ray detectors to that of the Li-glass flux monitor. We made use of the 4.9 eV resonance in ($^{197}Au+n$) in which capture strongly predominates over scattering. In an Au sample which is sufficiently thick (0.0029 atoms/b) so as not to appreciably transmit at resonance, the capture yield per unit neutron flux is evaluated. A Monte Carlo calculation was used to evaluate the neutron escape probability (~2.6%, primarily from back scattering). The independence of the measurement from the details of the capture gamma cascade had been previously verified by us to ~1% by the use of standards as diverse as the 6.7-eV resonance in ^{238}U and the 3.9-eV resonance in ^{165}Ho as well as the 4.9-eV resonance in ^{197}Au. (See also Yamamuro,[24] who has independently verified this independence using resonances in Ag, Au, and Ta.)

The processing of the $^{32}S(n,\gamma)$ data involved initially converting the time-of-flight data to energy dependent data, correcting for dead-time and time independent backgrounds (i.e., due to cosmic rays, radioactive contaminants in the material of construction, etc.). A second stage of processing involved sample-dependent and sample-independent beam induced background corrections. The sample independent background correction subtracts a normalized "no sample" run made under operating conditions similar to the foreground run. The fluorine in the fluorocarbon detector as well as the aluminum of the apparatus housing can give rise to capture gammas from neutrons scattered by the sample. These gammas contribute background dependent upon the sample thickness, the atomic mass of the sample constituents, and the sample's scattering cross section. The sample-dependent background correction is applied by constructing a background composed of both a $E^{-1/2}$ component and a resonance structure component from the known F and Al resonances that have been adjusted to a measured ^{208}Pb off-resonance spectrum. These second order effects are adequately taken into account here as judged by submillibarn residues in regions between resonances in a wide variety of samples.

The capture data have been analyzed with a least-squares fitting program[25] using the Breit-Wigner single-level expression

$$\sigma_\gamma = (\pi k^{-2}) \frac{g\Gamma_n\Gamma_\gamma}{(E-E_0)^2+(\Gamma/2)^2} \tag{9}$$

to extract the parameters E_0, Γ_n, and Γ_γ. Since the resonances seen in capture are narrow, both k and Γ_n were assumed constant and equal to their respective values at E_0. A "$1/v$" background term takes into account contributions from distant resonances. A field encompassing up to 500 data points and up to 15 resonances is evaluated at one time. The program iterates upon trial parameters applying corrections for systems resolution, Doppler width, resonance self-protection, and multiple scattering. Only the capture area $A=(2\pi^2/k^2)(g\Gamma_n\Gamma_\gamma/\Gamma)$ is determined when the resonance width is small compared to the resolution width ΔE. However, for cases in which the ratio, $\Gamma/\Delta E$, exceeds ~20% it is generally possible to also deduce the resonance width Γ, and these are found to be consistent with the more accurate values from the high resolution total cross section data.

A correction that may be required following the evaluation of the radiation width, Γ_γ^{exp}, concerns capture in the detector environment of neutrons scattered from discrete resonances in the sample. This prompt neutron sensitivity is generally small and can be formulated as a correction to Γ_γ that is proportional to Γ_n:

$$\Gamma_\gamma = \Gamma_\gamma^{exp} - c\Gamma_n. \tag{10}$$

Here c is dependent on the amounts and distribution of absorber in the environs of the detector. It is energy dependent and has been found to range from ~10^{-3} to ~10^{-4} over the energy range of this work. Values of c are considered accurate to ~30% and contribute to the uncertainty in Γ_γ only for the broadest resonances. The results of the capture resonance measurements are included with the results from the total cross section measurement in Table I. The energy scale used in Table I is from the better resolution total cross section measurement.

VI. RADIATION WIDTHS

The average total radiation widths of the five $s_{1/2}$, seven $p_{1/2}$, and eight $p_{3/2}$ resonances (Table

II) are 3.0(11) eV, 1.6(5) eV, and 0.72(20) eV, respectively. In all three cases, the dispersion of the observed radiation widths about their respective means implies three degrees of freedom for the assumed chi-squared distributions of the component partial widths. Such a small number of degrees of freedom implies that the γ cascade following capture is dominated by a few ($\approx$3) primary γ rays. This is consistent with the reported[12] capture γ-ray spectra for thermal and resonance (30 and $\approx$103 keV) neutron capture. These spectra are dominated by three or fewer primary transitions.

The average total radiation width for the eight $d_{5/2}$ resonances (Table II) is 0.78(15) eV and the dispersion of the total radiation widths implies 7 degrees of freedom for the assumed chi-squared distribution of partial radiation widths.

VII. THE CAPTURE KERNELS ($g\Gamma_n\Gamma_\gamma/\Gamma$) AND ASSIGNMENTS

Of the 64 resonances observed in this work, 13 have neutron widths too small to be seen in the transmission experiments. For these 13 and for 21 other narrow resonances, we report values for the capture kernel $g\Gamma_n\Gamma_\gamma/\Gamma$. In two instances, the resonances at 43.10 and 46.79 keV, the kernel is exceptionally small, i.e., $\approx\frac{1}{20}$ the average. This suggests, since the total radiation widths are not expected to vary by factors of 20, that in these two cases $\Gamma_\gamma \gg g\Gamma_n$, and the capture kernel reduces approximately to $g\Gamma_n$. Assuming Porter-Thomas distributions with the observed population averages for the s- and p-wave reduced neutron widths, the probabilities that these two resonances have $l=0$ or $l=1$ are $<0.1\%$ and $\approx 2\%$, respectively. Likewise, assuming that the f-wave average reduced neutron width is equal to that for the observed p-wave resonances, the probability that $l=3$ for either of these two resonances is much less than 0.1%. Hence, we suggest $l=2$ for both of these resonances. The capture spectrum for a resonance near 42 keV (neutron energy) is dominated[12] by one strong (66%) transition. If the $l=2$ assignment made here for the resonance at 43.1 keV is correct and if this is the same resonance seen in Ref. 12, then the decay of that d-wave resonance is typical compared to the 7 degrees of freedom for the other $d_{5/2}$ resonances listed in Table II.

VIII. DEDUCED CAPTURE WIDTHS AND CROSS SECTIONS

A. Thermal cross section and resonance integral

The observed[27] thermal capture cross section of 530 ± 10 mb cannot be accounted for by the contribution from the low energy $1/v$ tail of unbound s-wave resonances. Ignoring interference effects, the first s-wave resonance (102.7 keV) would contribute 135 mb and the higher energy s-wave resonances $\approx$1 mb. The remaining $\approx$394 mb of thermal cross section is presumably due to direct neutron capture and/or one or more bound levels. Mughabghab[28] has recently presented strong empirical evidence that the Lane and Lynn[29] model of direct neutron capture does correctly predict thermal cross sections in the mass range 40–50.

The expression for direct capture at thermal energy to a bound state with excitation energy E_μ with the emission of a γ ray of energy E_γ^μ is given by Lane and Lynn[29] as

$$\sigma_\gamma^\mu = \sigma_\gamma^\mu(\text{h.s.})\left(1+\frac{R-R'}{R}\,y_\mu\,\frac{y_\mu+2}{y_\mu+3}\right)^2, \tag{11}$$

where $y_\mu = k_\mu R$ and $k_\mu = (2mE_\gamma^\mu/\hbar^2)^{1/2}$ is the wave number of the neutron binding energy to the μth excited state. For the present case we assume that scattering in the tails of resonances far from thermal energy make negligible contribution to the direct capture, i.e., we take $R = R' \approx 4.1$ fm (see Ref. 16). The cross section for hard-sphere capture, the captured neutron going into an excited p state of ^{33}S, can be written[29]

$$\sigma_\gamma^\mu(\text{h.s.}) = \frac{0.062}{6R\sqrt{E_{\text{TH}}}}\left(\frac{Z}{A}\right)^2(2J+1)S_\mu\left(\frac{y_\mu+3}{y_\mu+1}\right)^2 y_\mu{}^2. \tag{12}$$

The spectroscopic factors S_μ (Table III) for the $l=1$ bound states in ^{33}S are from the work by Mermaz.[30] We assume that the primary intensities (Table III) following s-wave capture are as reported for an s wave near 111 keV by Bird *et al.*[12] (We obtain a more accurate energy 102.7 keV for this resonance.) The calculated thermal capture cross section is given by

$$\sigma_\gamma^{\text{cal}}(E_{\text{TH}}) = \sum_\mu |A_\mu^{\text{dir}} \pm A_\mu^{\text{res}} \pm A_\mu^B|^2 + 81 \text{ mb}, \tag{13}$$

where the 81 mb is due to capture in the 102.7-keV resonance leading to primary γ emission to $l\neq 1$ states in ^{33}S. The thermal capture amplitudes A_μ^{dir} (direct capture), A_μ^{res} (unbound resonance capture), and A_μ^B (bound resonance capture) are all taken as real.[29] All combinations of choices of relative phases for the amplitudes are apparently possible.

Calculations using Eq. (13) show that bound resonance capture is necessary to explain the observed thermal capture but the parameters for the bound state are uncertain. In Table III are presented the calculated thermal cross sections for four different assumptions. Columns labeled I and II present the results of assuming no bound level and both choices of relative phase. In both cases, the calculated

TABLE III. Contributions from direct, unbound, and bound resonances to the thermal capture cross section of $^{32}S+n$.

				Assumption			
				I	II	III [c]	IV [d]
E_μ (keV)	$(2J_\mu+1)S_\mu$ [a]	l_μ	$I\mu$ [b] (%)	$\lvert A_\mu^{dir}+A_\mu^{res}\rvert^2$ (mb)	$\lvert A_\mu^{dir}-A_\mu^{res}\rvert^2$ (mb)	$\lvert A_\mu^{dir}+A_\mu^{res}+A_\mu^{B}\rvert$ (mb)	$\lvert A_\mu^{dir}-A_\mu^{res}-A_\mu^{B}\rvert^2$ (mb)
3221	1.90	1	30	245	9	338	419
4213	0.30	1	<1	12	12	12	12
4920	0.088	1	<1	3	3	3	3
5715	1.06	1	10	84	3	84	3
5894	0.44	1	<1	12	12	12	12
			$\sum=$ 40	$\sum=$ 356	$\sum=$ 39	$\sum=$ 449	$\sum=$ 449
...	...	$l\neq1$	60	81	81	81	81
			$\sigma_\gamma^{cal}(E_{TH})$	437	120	530	530

[a] Spectroscopic factors taken from Ref. 29.
[b] Primary γ intensities taken from Ref. 12.
[c] Assumed s-wave bound level at −319 keV with $\Gamma_\gamma=3$ eV and $\Gamma_n^0=15$ eV.
[d] Assumed s-wave bound level at −38 keV with $\Gamma_\gamma=3$ eV and $\Gamma_n^0=15$ eV.

thermal cross section is smaller than the reported value. The columns labeled III and IV present the results of placing a bound level with reduced neutron width $\Gamma_n^0=15$ eV and $\Gamma_\gamma=3.0$ eV (the average widths for the five s-wave resonances) so as to account for the observed thermal cross section. It is arbitrarily assumed that the bound state capture goes only to the 3221-keV excited state (such an assumption is consistent with the thermal spectrum[12]). For assumption III, all amplitudes in phase, the bound resonance would be located at $E_0=-319$ keV. For assumption IV, the resonance amplitudes out of phase with respect to those for direct capture, the bound resonance would be at $E_0=-38$ keV. These results are presented only as examples of the many possibilities for satisfactory accounting for the observed thermal capture cross section.

B. The resonance integral

The neutron capture resonance integral $I=\int_{0.5\,eV}^{1.1\,MeV}\sigma_c dE/E$ of sulfur is of interest for estimating reaction rates in thermal nuclear reactors and concrete shielding. The resonance integral of ^{32}S attributable to the $1/v$ components (direct capture and bound level) of the cross section is 239 mb and that deduced from unbound resonances is 11 mb, giving a total resonance integral of 250 mb. This low value reflects the large value of $\langle D_0\rangle$ and especially the absence of resonances at low energies.

C. Maxwellian-averaged cross sections at stellar temperatures

The capture of neutrons by ^{32}S in stellar interiors is one of several reactions involving ^{32}S during element buildup. Of interest in this connection are neutron capture cross sections averaged over Maxwellian energy distributions for temperatures characteristic of stars supporting the s process (say 10^8–10^9 °K). In Fig. 7 is shown a plot of the Maxwellian-averaged cross section $\bar{\sigma}_\theta=\langle v\sigma\rangle/v_\theta$ for a range of energies (i.e., temperatures $E_\theta=kT$) of importance in astrophysical process. The resonances at $30.38(\frac{1}{2}^-)$ and $102.7(\frac{1}{2}^+)$ keV are the two largest contributors to the Maxwellian-averaged cross section. In particular, the value of $\bar{\sigma}_\theta=4.2(2)$ mb for $E_\theta=30$ keV reflects the sharp reso-

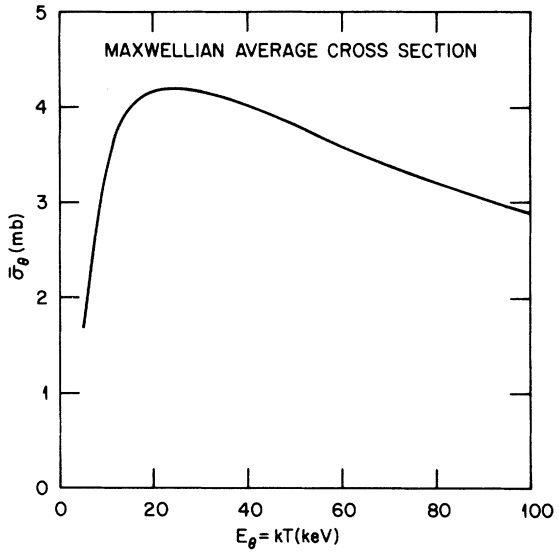

FIG. 7. The Maxwellian average cross section is shown for neutron temperatures from 5 to 100 keV. The 4.2(2) mb cross section at 30 keV strongly reflects the presence of the resonance at 30.38 keV.

nance at 30.38 keV. The cross section $\bar{\sigma}_\theta$ exhibits a broad maximum at ~30 keV making the reaction insensitive to stellar temperature over variations of a factor of 2 in either direction. Allen *et al.*[31] have reported $\bar{\sigma}_\theta = 3.0$ mb for 30-keV neutrons based on less nearly complete data than reported here.

D. Valency model radiation widths

Evidence has been presented by Allen and Musgrove[32] that shell model single-particle contributions (i.e., single neutron transitions first suggested by Lane and Lynn[28]) to neutron resonance capture become significant and may even dominate in the mass regions at and above the neutron closed shells and correlate well with the neutron strength function peaks.

We have calculated the valency contribution ($\Gamma_\gamma{}^v$) to the radiation widths of $s_{1/2}$, $p_{1/2}$, $p_{3/2}$, and $d_{5/2}$ resonances in the $^{32}S + n$ system and compared them to our measured values Γ_γ. The partial radiation width for a resonance λ decaying to a final state μ in valency capture, assuming electric dipole de-excitation, can be written as[32]

$$\Gamma_{\gamma\lambda\mu} = q_{\lambda\mu}(E_\gamma) S_\mu \Gamma^l_{n\lambda} E_\gamma{}^3 (Z^2/A^2) . \qquad (14)$$

Here $q_{\lambda\mu}(E_\gamma)$ is the overlap integral including orientation effects, S_μ is the (d,p) spectroscopic factor of the final state, $\Gamma^l_{n\lambda}$ is the reduced neutron width of the initial state, and E_γ is the energy of the primary gamma. The energy dependent $q_{\lambda\mu}(E_\gamma)$ term has been evaluated by Allen and Musgrove[32] for transitions of interest and the spectroscopic factors for $^{32}S(d,p)^{33}S$ are from Ref. 30. The capture gamma spectrum for ^{32}S has been studied[12,33] and the level scheme is well established.[34] By summing the calculated partial widths to the low lying final states we have estimated the valency contribution in 28 resonances. In Table II are listed the radiation widths and the ratios of the calculated valency width to the observed width for several J^π groups. Of the five s-wave resonances, only for the very large resonance at 102.7 keV is the valency contribution appreciable; the average value of the calculated s-wave valency contribution is $\langle \Gamma_\gamma{}^v/\Gamma_\gamma^{obs} \rangle = 0.070$ (see Table II). Similarly for eight resonances that have been unambiguously identified as $d_{5/2}$, we calculate an average $\langle \Gamma_\gamma{}^v/\Gamma_\gamma^{obs} \rangle = 0.10$. Thus the valency capture mechanism seems to play a minor role in the capture for the positive parity states. This conclusion is consistent with the conjectures of Allen and Musgrove.[32]

An examination of the average valency components $\Gamma_\gamma{}^v$ of the seven $p_{1/2}$ resonances gives a value of $\langle \Gamma_\gamma{}^v/\Gamma_\gamma^{obs} \rangle = 0.50$. The strong resonance at 202.6 keV contributes heavily to the average and represents what may be experimental evidence for destructive interference between the valency and other capture mechanisms. However, even excluding that resonance, the average ratio $\langle \Gamma_\gamma{}^v/\Gamma_\gamma^{obs} \rangle = 0.36$. This result is consistent with but by no means proves the importance of the valency mechanism in $p_{1/2}$ resonance capture in ^{32}S. Testing for the correlation between $\Gamma^0_{n\lambda}$ and $\Gamma_{\gamma\lambda\mu}$ predicted by the valency model would provide definitive evidence for valency capture but requires the partial radiation widths rather than the total widths which we have measured.

Valency contributions for eight $p_{3/2}$ resonances give an average ratio $\langle \Gamma_\gamma{}^v/\Gamma_\gamma^{obs} \rangle = 0.13$, only slightly greater than that for the positive parity resonances. The $p_{3/2}$ single-particle state in ^{32}S is considerably more tightly bound than the $p_{1/2}$ state, and hence the expected $p_{3/2}$ valency component would be smaller since the overlap integral is relatively smaller.[35]

IX. UNBOUND LEVELS IN ^{33}S

Resonance properties of $(^{32}S + n)$ determined in this experiment are compared in Table IV with measurements in which other reactions have been used to excite levels in ^{33}S in the energy region studied here, $E_{exc}(^{33}S) = 8640$–9700 keV or $E_n(\text{lab}) = 0$–1100 keV. Levels excited in (d,p) stripping [energy threshold $E_{exc}(^{33}S) = 6419$ keV] may be correlated with those measured in the neutron experiments. Liljestrand *et al.*[36] report angular distributions and l assignments for 18 resonances derived from (d,p) stripping up to 9460 keV of excitation. Although the uncertainty in the excitation energy of ±10 keV makes an unambiguous matching of levels difficult, seven resonances reported in our work (see Table IV) [8671.7($\frac{1}{2}^-$), 8741.8($\frac{1}{2}^+$), 8838.7($\frac{1}{2}^-$), 9007.3($\frac{1}{2}^+$), 9211.2($\frac{5}{2}^+$), 9317.1($\frac{1}{2}^+$), and 9402.1($l>1$) keV] can be identified with levels assigned by Liljestrand. For three levels [9031.1($l>0$), 9139.9($l>0$), and 9287.9($l>0$) keV] for which we can assign only lower limits for l, Liljestrand *et al.* makes the assignments $l = 2$, 2, and 3, respectively. Three f-wave resonances were seen only by Liljestrand *et al.* (8729, 8873, and 9245 keV). Due to the small f-wave penetrabilities these resonances would not be expected to be seen in our neutron experiments. The d-wave level reported by Liljestrand *et al.* at 8644 keV would similarly not be expected to be seen in the neutron work, and in fact the large uncertainty in that energy is consistent with a bound level. Their p-wave assignment to a level at 9460 keV with a large width appears to be contradicted by the absence of such a level in the neutron data.

TABLE IV. Comparison with other work.

$E_{exc}(^{33}S)$ (keV)	J^{π} or l	Reference 36 E_{exc} (keV)	Reference 36 l	Reference 37 E_{exc} (keV)	Reference 37 l	Reference 38 E_{exc} (keV)	Reference 38 l
...	...	8644	2				
8671.7	$\frac{1}{2}^-$	8670	1	8673	(0,1)		
8684.0	($l=2$)			8690	>2		
8687.6	($l=2$)						
		8729	3				
8736.7	$\frac{3}{2}^-$						
8741.8	$\frac{1}{2}^+$	8749	0	8752	0		
8751.0	$\frac{3}{2}^-$						
8782.9							
8797.5	$l=1,2$						
8809.7							
8838.7	$\frac{1}{2}^-$	8838	(1,3)	8839	1		
		8873	3				
8895.3	$l>0$						
8906.0	$\frac{1}{2}^-$			8910	1		
8921.8	$\frac{3}{2}^-$			8926	1		
8941.9	$l>0$	8939	3	8942	>1	8942	
8945.1							
8953.6							
8977.5	$l>0$	8975	3	8973	>1		
8984.7	$l>0$						
9007.3	$\frac{1}{2}^+$	9005	0	9010	0		
9009.2							
9012.7							
9031.1	$l>0$	9035	2				
9042.0	$\frac{3}{2}^-$						
9055.1							
9087.9	$l>1$					9071	
9090.9	$\frac{5}{2}^+$	9115	...				
9139.9	$l>0$	9138	2				
9159.0	$l>0$	9175	...				
9200.8							
9210.6	$l>0$						
9211.2	$\frac{5}{2}^+$	9209	2	9211	2	9213	
		9245	3				
9268.0							
9271.7	$\frac{5}{2}^+$						
9287.9	$l>0$	9280	3			9288	

TABLE IV. *(Continued.)*

		Reference 36		Reference 37		Reference 38	
$E_{exc}(^{33}S)$ (keV)	J^{π} or l	E_{exc} (keV)	l	E_{exc} (keV)	l	E_{exc} (keV)	l
9297.0	$\frac{5}{2}^+$						
9309.2							
9317.1	$\frac{1}{2}^+$	9320	0	9318	0		
9344.9	$\frac{1}{2}^-$	9350	3	9348	1		
9357.6							
9360.5	$\frac{3}{2}^-$			9363	1	9362	
9395.0	$l>0$						
9397.2	$\frac{3}{2}^-$						
9402.1	$l>1$	9400	2	9400	2	9403	
9436.0	$\frac{5}{2}^+$			9436	2	9442	
9450.6	$l>1$						
		9460	1				
9481.5	$l>0$					9470	
9484.6	$l>0$						
9499.9	$l>1$					9499	
9515.9	$l>1$						
9524.3							
9534.0	$\frac{5}{2}^+$					9531	
9534.9	$\frac{3}{2}^-$			9539	1		
9560.6	$\frac{5}{2}^+$			9564	2	9571	
9597.1	$\frac{1}{2}^-$						
9619.4	$l>0$						
				9607	0		
9619.4	$\frac{1}{2}^-$						
9655.2	$l>0$						
9656.7	$\frac{1}{2}^+$						
9658.7	$\frac{1}{2}^-$						
9665.4	$\frac{5}{2}^+$			9666	1		
9671.7							
9674.6	$\frac{1}{2}^+$					9675	
9693.4	$l>1$						
9700.4	$\frac{3}{2}^-$					9699	1

Bommer *et al.*[37] pointed out that the much greater efficiency in exciting higher angular momenta in the (d,p) reaction as compared with exciting identical states in (n,n) scattering can yield l assignments. Integrating the cross section over the resonance for each type of experiment and forming the ratio

$$\int \sigma(d,p)dE \Big/ \int \sigma(n,n)dE$$

produces a parameter independent of the reduced width of the resonance. Penetrability effects (primarily in the neutron channel) produce an expected enhancement of up to one order of magnitude in

this ratio for each added unit of angular momentum transferred. By comparing their (d,p) data with the total neutron cross section data of Peterson[8] and adopting level energies from Peterson, Bommer *et al.* assigned l values to 19 resonances in our energy region (Table IV). Bommer's assignments agree with ours for 15 of these resonances [8671.7($\frac{1}{2}^-$), 8684.0($l=2$), 8741.8($\frac{1}{2}^+$), 8838.7($\frac{1}{2}^-$), 8906.0($\frac{1}{2}^-$), 8921.8($\frac{3}{2}^-$), 9007.3($\frac{1}{2}^+$), 9211.2($\frac{5}{2}^+$), 9317.1($\frac{1}{2}^+$), 9344.9($\frac{1}{2}^-$), 9360.5($\frac{3}{2}^-$), 9402.1($l=2$), 9436.0($\frac{5}{2}^+$), 9534.9($\frac{3}{2}^-$), and 9560.6($\frac{5}{2}^+$) keV]. Two resonances cannot be correlated with resonances seen in our neutron work. In particular, Bommer's assignment of $l=0$ to a resonance at 9607 keV with $\Gamma_n=20$ keV must be in error, since such a resonance would be easily detected in our work. (Note the s-wave resonance with width $\Gamma_n=2.1$ keV seen in this work at excitation energy 9656.7 keV.) Bommer's assignment of $l=1$ for the 9666 level is contradicted by our value of $J^\pi=\frac{5}{2}^+$. It would appear that Peterson's resolution would have been inadequate to resolve the two resonances seen in our work at 9658.7($\frac{1}{2}^-$) keV and 9665.4($\frac{5}{2}^+$) keV; hence Bommer would have treated this doublet as a single resonance in his analysis. Bommer's assignment of $l>1$ for the two levels at 8942 and 8973 keV is consistent with the $l>0$ suggested from our neutron work.

The $^{29}Si(\alpha,n)^{32}S$ reaction has been used to excite levels in ^{33}S. Balakrishnan *et al.*[38] report 13 resonances (Table IV) in the region of interest with an energy uncertainty of 5 keV. Ten of these are sufficiently close in energy to be identified with levels seen in the present work. McMurray *et al.*[39] have measured the angular neutron distribution for the state at 9700 keV and deduced $J=\frac{3}{2}$ in agreement with the $\frac{3}{2}^-$ assignment from the (n,n) experiment. The $^{32}S(n,\alpha)^{29}Si$ reaction is exoergic by 1525 keV. However, the Coulomb barrier for the alpha channel implies relatively low cross sections below 1 MeV neutron energy. By use of the reciprocity theorem, resonance (n,α) cross sections can be deduced from the (α,n) measurements. Balakrishnan reports $\sigma_0(\alpha,n)\approx 33$ mb for the peak cross section of the $E_n=1091$ keV resonance; and somewhat smaller cross sections can be deduced for the lower energy resonances that he reports. This implies alpha widths comparable to or somewhat larger than the radiative widths for neutron energies above $E_n\simeq 500$ keV and less than 1000 keV. The $^{32}S(n,p)^{32}P$ reaction is endoergic by 928 keV and that channel need not be considered in our energy region.

X. CONCLUSIONS

The present investigation approximately triples the number of known resonances in $^{32}S+n$ below neutron energy 1.1 MeV. Many of the newly found resonances are quite narrow but, even so, resonance parameters were derived from high resolution transmission and capture data for most of them. The J^π assignments reported in this paper are generally consistent with, but more nearly certain than, those from earlier work. Many of the remaining uncertain J^π assignments could be resolved by high resolution neutron scattering measurements. Extension of the present work to higher energies will require multilevel R-matrix analysis. We find that the valence capture mechanism may play an appreciable role in the capture process only for the $p_{1/2}$ resonances. Direct capture does seem to make a significant contribution to the thermal capture cross section.

ACKNOWLEDGMENTS

We are grateful to Dr. J. A. Harvey and N. W. Hill for their essential help and guidance in the measurement of total cross sections. This research was sponsored by the Division of Basic Energy Sciences, U. S. Department of Energy, under Contract No. W-7405-eng-26, with the Union Carbide Corporation.

---

*Present address: Denison University, Granville, Ohio.

[1]R. K. Adair, C. K. Bockelman, and R. E. Peterson, Phys. Rev. 76, 308 (1949).
[2]R. O. Lane, A. S. Langsdorf, Jr., J. E. Monahan, and A. J. Elwyn, Ann. Phys. (N.Y.) 12, 135 (1961).
[3]J. B. Garg, J. Rainwater, S. Wynchank, and W. W. Havens Jr., in Proceedings of the International Conference on the Nuclear Structure of Neutrons, Antwerp, 1965 (unpublished), p. 74.
[4]U. N. Singh, J. B. Garg, J. Rainwater, W. W. Havens, Jr., and S. Wynchank, Report No. INDC(USA)-35 "U", 1971 (unpublished), p. 74.
[5]S. Wynchank, F. Rahn, H. S. Carmada, G. Hacken, M. Slagowitz, H. I. Liou, J. Rainwater, and W. W. Havens, Jr., Nucl. Sci. Eng. 51, 119 (1973).
[6]R. L. Macklin, P. J. Pasma, and J. H. Gibbons, Phys. Rev. B 136, 695 (1964).
[7]R. E. Peterson, H. H. Barschall, and C. K. Bockelman, Phys. Rev. 79, 593 (1950).
[8]S. Cierjacks, P. Forti, D. Kopsch, L. Kropp, J. Nebe, and H. Unseld, Kernforschungszentrum Karlsruhe Report No. EANDC(E)-111 "U", 1968 (unpublished).
[9]R. C. Block, Bull. Am. Phys. Soc. 12, 512 (1967).
[10]I. Bergqvist, J. A. Biggerstaff, J. H. Gibbons, and W. M. Good, Phys. Rev. 158, 1049 (1967).
[11]B. Lundberg and I. Bergqvist, Phys. Scr. 2, 265 (1970).

[12]J. R. Bird, B. J. Allen, I. Bergqvist, and J. A. Biggerstaff, Nucl. Data Tables 11, 456 (1973).
[13]C. H. Johnson, J. L. Fowler, and N. W. Hill, Bull. Am. Phys. Soc. 18, 538 (1973).
[14]D. C. Larson, C. H. Johnson, J. A. Harvey, and N. W. Hill, ORNL Report No. ORNL-TM-5612, 1976 (unpublished).
[15]A. M. Lane and R. G. Thomas, Rev. Mod. Phys. 30, 2 (1958); 30, 257 (1958). See pages 302-324.
[16]S. F. Mughabghab and D. I. Garber, BNL Report No. BNL-325, Third Edition (1973), Vol. 1, p. xxii.
[17]R. L. Macklin, Nucl. Instrum. Methods 91, 79 (1971).
[18]R. L. Macklin and J. H. Gibbons, Phys. Rev. 159, 1007 (1967).
[19]B. J. Allen, R. L. Macklin, R. R. Winters, and C. Y. Fu, Phys. Rev. C 8, 1504 (1973).
[20]C. A. Uttley *et al.*, USAEC Report No. CONF710301, 1971 (unpublished).
[21]W. P. Poenitz, Z. Phys. 268, 359 (1974).
[22]E. Fort, J. P. Marquette, M. S. Coates, G. J. Hunt, and C. A. Uttley, in Proceedings of the Second International Atomic Energy Agency Panel on Neutron Standard Reference Data, Vienna, 1972 (unpublished).
[23]R. L. Macklin and J. Halperin, Phys. Rev. C 11, 1270 (1975), Appendix 1.
[24]N. Yamamuro, T. Hayase, T. Doi, Y. Fujita, K. Kobayashi, and R. C. Block, Nucl. Instrum. Methods 133, 53 (1976).
[25]R. L. Macklin, ORNL Report No. ORNL-TM-4810, 1975 (unpublished).
[26]J. Rainwater, W. W. Havens, Jr., C. Wu, and J. R. Dunning, Phys. Rev. 73, 733 (1948).
[27]A. DeVolpi and K. G. Porges, Bull. Am. Phys. Soc. 13, 1421 (1968), corrected for minor isotope contributions.
[28]S. F. Mughabghab, Phys. Lett. 81B, 93 (1979), No. 12.
[29]A. M. Lane and J. E. Lynn, Nucl. Phys. 17, 563 (1960).
[30]M. C. Mermaz, C. A. Whitten, Jr., J. W. Champlin, A. J. Howard, and D. A. Bromley, Phys. Rev. C 4, 1778 (1971).
[31]B. J. Allen, J. H. Gibbons, and R. L. Macklin, in *Advances in Nuclear Physics*, edited by Baranger and Vogt (Plenum, New York, 1971), Vol. 4, Chap. 4.
[32]B. J. Allen and A. R. de L. Musgrove, in *Advances in Nuclear Physics*, edited by Baranger and Vogt (Plenum, New York, 1978), Vol. 10, Chap. 2.
[33]G. A. Bartholomew, A. Doveika, K. M. Eastwood, S. Monaro, L. V. Groshev, A. M. Demidov, V. I. Pelekhov, and L. L. Sokolovskii, Nucl. Data A3, 367 (1967).
[34]P. M. Endt and C. Van der Leun, Nucl. Phys. A310, 1 (1978).
[35]H. Weigmann, S. Raman, J. A. Harvey, R. L. Macklin, and G. G. Slaughter, in *Proceedings of the Third International Symposium on Neutron Capture Gamma-Ray Spectroscopy and Related Topics*, edited by R. E. Chrien and W. E. Kane (Plenum, New York, 1979), pp. 797–799.
[36]R. Liljestrand, J. McIntyre, G. Planpied, J. Lynch, L. Ray, W. R. Coker, and G. W. Hoffman, Phys. Rev. C 11, 1570 (1975).
[37]J. Bommer, M. Ekpo, H. Fuchs, K. Grabisch, H. Kluge, and H. Oschler, Nucl. Phys. A263, 93 (1976).
[38]M. Balakrishnan, M. K. Mehta, A. S. Divatia, and S. Kailas, Phys. Rev. C 11, 54 (1975).
[39]W. R. McMurray, D. M. Holz, I. J. van Heerden, and G. Wiechers, Z. Phys. 247, 453 (1971).